JOURNAL OF SOLID STATE CHEMISTRY 103, 490–503 (1993)

Structural Study of Lead Orthophosphovanadates: Role of the Electron Lone Pairs in the Phase Transitions

JEAN-MICHEL KIAT,*†‡ PIERRE GARNIER,*
GILBERT CALVARIN,* AND MARCEL PINOT†

Laboratoire de Chimie-Physique du Solide, URA au CNRS No. 453, Ecole Centrale de Paris, 92295 Châtenay-Malabry Cedex, France, and †Laboratoire Léon Brillouin, CEN Saclay, 91191 Gif-sur-Yvette Cedex, France

Received May 5, 1992; in revised form September 28, 1992; accepted October 2, 1992

A structural investigation of the lead orthophosphovanadate compounds $Pb_3P_{2x}V_{2(1-x)}O_8$ has been performed using neutron and X-ray powder diffraction. Results obtained by a Rietveld analysis are presented and compared with previous data on "pure" lead vanadate ($x = 0$) and lead phosphate ($x = 1$). The influence of the substitution of phosphorus for vanadium on the mechanism of the phase transitions of lead vanadate and lead phosphate is analyzed. For a given concentration x, a decrease of the distance between the layers of lead atoms is observed when the temperature diminishes. In the vanadium- and phosphorus-rich compounds a critical value is reached where the lone pairs of the lead atoms repel each other as well as the proximate oxygen atoms: this induces a phase transition from the high temperature phase. For the other compounds (middle part of the phase diagram) a critical value is not reached and the high temperature phase remains stable down to 5 K. The possibility of a monoclinic local order inside the high temperature rhombohedral phase is also pointed out.

Introduction

Lead orthophosphate, $Pb_3(PO_4)_2$ (or $Pb_3P_2O_8$), and lead orthovanadate, $Pb_3(VO_4)_2$ (or $Pb_3V_2O_8$), display ferroelastic phase transitions from a common high temperature rhombohedral γ-phase $R\bar{3}m$ ($Z = 1$) to different monoclinic phases (Fig. 1). $Pb_3P_2O_8$ transforms at 453 K into a β'-phase with a space group which was for a long time reported to be $C2/c$ ($Z = 4$); however, we have recently shown the existence of a very weak noncentrosymmetry (the exact space group is $C2$, $Z = 4$) which will not be considered in this paper, the largest displacement between the centrosymmetric and the noncentrosymmetric structural models being below 0.03 Å (*1*). $Pb_3V_2O_8$ transforms at 373 K into a β-phase with $P2_1/c$ ($Z = 2$) space group, and at 273 K into an α phase with $A2$ ($Z = 2$) space group (the exact space group of the α-phase, first determined by powder sample studies (*2*), was recently confirmed by expériments on single crystals (*3*)). An analogy with the martensitic transformations has been proposed (*4*): (i) as in metals and alloys, the transformations are strongly first order with important shears and large phase coexistences; (ii)

‡ Author to whom correspondence is to be addressed.

0022-4596/93 $5.00

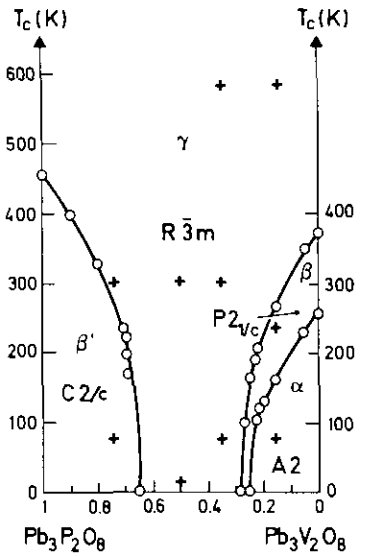

FIG. 1. Critical temperatures versus concentrations x phase diagram of the $Pb_3P_{2x}V_{2(1-x)}O_8$ orthophosphovanadate compounds from a single crystal study (Ref. (4)). The critical temperatures can be slightly different for powdered samples of the mixed compounds, due to huge phase coexistence and hysteresis. The crosses are the concentration and temperature points investigated in this study.

they progress through the crystal by moving a planar stress free interface (habit plane); (iii) they possess an unusual pretransitional mechanism (5) which is very similar to the so-called premartensitic regime (6).

We have recently reported a Rietveld analysis of the three phases of lead vanadate and have compared them with the two phases of lead phosphate (7). We have emphasized the stereochemical influence of the electronic lone pair of Pb^{II} ions on the phase transitions and have given a structural explanation for the martensitic-like behavior. Indeed in the common γ-rhombohedral phase the structure is a stacking of PO_4 or VO_4 tetrahedra layers, orthogonal to the threefold axis (Fig. 2). In a layer, chains of tetrahedra are connected by lead atoms of two types: Pb_1 inside the layers and Pb_2 at the surfaces of the layers. In the γ, β', and β phases the Pb_1^{II} ions are located on centrosymmetric sites and consequently the electronic lone pair remains centered on the nucleus; in the case of the Pb_2^{II} ions, which are located on noncentrosymmetric sites for all phases, the center of the steric space occupied by the electronic lone pair does not coincide with the nucleus of the Pb^{II} ion. These lone pairs occupy the interlayers (d_i) and weakly connect the layers of tetrahedra. We have shown that the different monoclinic phases that appear from the γ-common rhombohedral phase differ mainly in the direction of tilting of the lone pair of the Pb_2^{II} ion taking place at the critical temperatures. The main displacements observed at the phase transitions are those of the Pb_2 atoms parallel to the layers. This explains

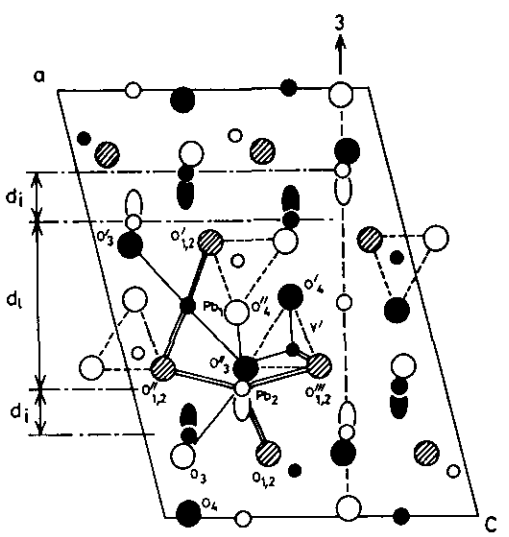

FIG. 2. Projection of the structure of the rhombohedral γ-phase of $Pb_3V_2O_8$ in the monoclinic a, c plane of the common cell (this cell is used to compare all the different phases of the mixed system; see text). The small, medium, and large circles represent respectively the vanadium, lead, and oxygen atoms, and the lobes represent the electron lone pairs. Open circles are located at $y = \frac{1}{4}$, closed circles at $y = \frac{3}{4}$, and hatched circles at $y \approx 0$ and $\approx\frac{1}{2}$. The VO_4 tetrahedra are represented by dashed lines; d_l and d_i are the layer thickness and interlayer distances, respectively (from Ref. (7)).

the possibility of strong shears of the structures as in metals and alloys.

It is possible to synthesize mixed compounds $Pb_3P_{2x}V_{2(1-x)}O_8$ in the whole range of concentration $0 \leq x \leq 1$. The influence of the substitution on the phase transitions of the two "pure" compounds was reported and the phase diagram of this system has been determined (Fig. 1) (*4*). Its main characteristics are (i) the existence of a common γ rhombohedral phase whatever x is; (ii) a rapid decrease of critical temperatures with x; (iii) an absence of phase transitions in the middle part of the diagram; (iv) no change of the order of the transitions (no tricritical point) but a huge increase of the phase coexistence (with a temperature range up to more than 100°), the transformed and nontransformed phases coexisting down to 5 K for the highly substituted compounds.

In order to understand the structural consequences of the substitution of phosphorus for vanadium we report in this paper a Rietveid analysis for different mixed compounds, $x = 0.15$, 0.35, 0.5, and 0.75, at several temperatures (Fig. 1) and compare the results with the existing data for $x = 0$ and $x = 1$ (*7*, *8*). The aim of this paper is to improve the understanding of the phase diagram of this system by analyzing the consequences of the substitution for the stereochemical behavior of the electronic lone pairs in the structural transitions.

Experimental and Refinements

Well-crystallized powder samples were synthesized by mixing PbO, V_2O_5, and $NH_4H_2PO_4$ in the appropriate proportions and melting them in a platinum crucible at 1000°C in air for 1 hr. The melt was cooled (100 K hr^{-1}) down to room temperature. After being ground the samples were annealed at 700°C for 12 hr.

For $x \leq 0.35$ neutron diffraction experiments were performed at the Léon Brillouin Laboratory using the Orphée reactor facilities (Saclay, France) on the two-axis diffractometer 3T2 with a wavelength of 1.226 Å. The patterns were scanned through steps of 0.05° between 6° and 110° (2θ) with a counting time by step of 60 s. For $x \geq 0.5$ neutron diffraction investigations were conducted on the high resolution D2B diffractometer with a wavelength of 1.5946 Å, attached to the Institut Laue–Langevin in Grenoble, France. The data were recorded by steps of 0.025° between 0 and 160° (2θ) with a counting time by steps of 10 sec. In both cases the sample was placed in a vanadium can. For the low temperature experiments a He cryostat with thermal stability of 0.1 K and precision within 1 K was used.

To get information regarding the atomic positions of vanadium inside the common γ rhombohedral phase we also performed for this phase X-ray diffraction studies using a two axis diffractometer (Bragg–Brentano geometry) with Cu$K\bar{\alpha}$ monochromatic radiation from an 18 kW Rigaku rotating anode (*9*). The patterns were scanned through steps of 0.01°, between 12° and 100° (2θ), with a counting time by steps of 15 sec. The thermal stability and precision of the cryostat were the same as in the neutron experiments and for the high temperature experiments a Rigaku furnace was used with stability of 1 K and precision of 2 K.

Least squares structure refinements were performed with the Rietveld analysis program DBW3.2 (*10*). In the γ $R\bar{3}m$ common cell there are one lead atom Pb(1) in the "a" special Wyckoff position, one lead atom Pb(2), one phosphorus or vanadium atom, one oxygen atom O(1) in the special "c" position, and one oxygen atom O(4) in general position. The starting values were the atomic coordinates obtained from reference (*7*). In the β ($P2_1/c$) and α ($A2$) cells there is one lead atom Pb(1) in the "a" special Wyckoff position; all the other atoms (one lead Pb(2), one phosphorus or vanadium, and four oxygen atoms) are in general positions. In the β' ($C2/c$) cell there is one Pb(1)

in the "*e*" special position; all the other atoms are in general positions. Partially substituted sites with weight x and $1 - x$, respectively, were used for the phosphorus and vanadium atoms with their corresponding form factors and scattering lengths.

The background intensity was measured on the patterns out off the Bragg peaks and interpolated between these values. In a first step we deduced from the neutron data (for which Gaussian lineshapes were satisfactorily used) the positions of lead, oxygen, and phosphorus atoms. In a second step the positions of lead and phosphorus atoms were again refined from the X-ray data (using pseudo-Voigt lineshape) but they show no significant deviations ($<2\sigma$) from those obtained in the neutron refinements. In a third step the positions of the vanadium atoms were refined from the X-ray data.

The number of refined structural parameters, the values of the different R reliability factors, and the refined cell parameters are listed in Table I. The reported R values for the neutron refinements are quite satisfactory, and those of X-ray refinements are only fair because of classic difficulties with the definition of the profiles due to the good resolution (typically 25 $10^{-3\circ}$ (2θ)) which is sensitive to anisotropic broadening. For the $x = 0.15$ compound the R_{wp} factors are of the same order as those observed for lead vanadate $x = 0$ in the same experimental conditions (*7*) whereas for the other compounds the reliability factors are less good, particularly in the γ phase at low temperature ($x = 0.35$, 0.5) (this point will be discussed later).

Results

The refinements were carried out utilizing the symmetries of the cells reported in Table I and the corresponding refined atomic positions and the isotropic temperature factors (B) are reported in Table II. However, comparisons between different structures is much easier using a common monoclinic cell, which is that of the β'-phase (rich in phosphorus compounds). In the rhombohedral phase this common cell is all face centered (F) in addition to algebraic relationships between the monoclinic parameters due to the threefold symmetry ($c = b\sqrt{3} = 3\,a \cos\beta$). In the β' and β-phases only the C and A faces, respectively, remain centered, whereas in the α phase the common cell is again all centered (F) but without the relationships between the cell parameters. The principal bond distances are reported in Tables III and IV.

The neutron and X-ray diffraction refinements show no evidence of phosphorus/vanadium ordering in the structures. Moreover we have tested the possibility of coexistence, in the γ phases, of two different types of tetrahedra, PO_4 and VO_4, with different sizes. This was done, in addition to the phosphorus/vanadium partially substituted atoms, by splitting each of four oxygen atoms of the tetrahedra into two oxygen atoms with weights x and $1 - x$. No significant change in positions, as well as no improvement in the R values, was obtained with this split-atom model.

From a global point of view it can be noted that: (i) The evolution of atomic coordinates and interatomic distances occurring during the different transitions for the $x = 0.15$ and 0.75 compounds are similar to the evolutions observed previously for lead vanadate ($x = 0$) and lead phosphate (*7*, *8*, *1*). (ii) For the compositions ($x = 0.35$ and 0.5) for which no transition is observed the atomic coordinates remain remarkably constant down to 5 K. (iii) For the rhombohedral phases high values for the B thermal factor are observed, particularly at low temperature and principally for the Pb^{II} ion (for instance $B = 5.07$ Å^2 at 5 K for the $x = 0.5$ compound). (iv) For the β and β'-phases the B values are lower but important for the considered temperature. (v) For the α low temperature phase the values of the B ther-

TABLE I

AGREEMENT FACTORS AND REFINED CELL PARAMETERS (Å)

Composition (x):	0.15			0.35			0.50		0.75	
Temperature (K):	85	235	585	85	300	585	5	300	85	300
Space group:	$A2$	$P2_1/C$	$R\bar{3}m$	$R\bar{3}m$	$R\bar{3}m$	$R\bar{3}m$	$R\bar{3}m$	$R\bar{3}m$	$C2/C$	$R\bar{3}m$
					Neutron					
N	25	25	11	11	11	11	11	11	26	11
R_p(%)	4.55	4.56	4.67	5.87	4.97	5.28	7.40	5.77	6.05	6.44
R_{wp}(%)	5.88	5.88	5.88	8.14	6.91	7.00	11.10	8.08	7.82	8.73
R_{exp}(%)	2.10	2.11	2.45	2.48	1.80	2.63	1.05	1.06	1.08	1.11
R_B(%)	2.28	2.29	3.93	4.24	3.65	3.36	4.30	3.34	3.43	4.02
a(Å)	7.4532(3)	7.5075(4)	5.7368(3)	5.6739(1)	5.6712(4)	5.6904(3)	5.6434(3)	5.6441(2)	13.8245(5)	5.5974(2)
b(Å)	6.1641(3)	6.0493(4)							5.7616(2)	
c(Å)	9.3094(4)	9.4814(4)	20.4615(10)	20.3412(10)	20.3804(11)	20.4702(11)	20.3373(8)	20.4031(6)	9.4908(3)	20.3733(6)
β(°)	116.149(3)	115.162(3)							102.265(2)	
					X-rays					
N			7	7	7	7		7		7
R_p(%)			9.00	9.00	9.19	9.00		9.48		10.66
R_{wp}(%)			12.54	12.79	12.91	12.54		2.78		2.81
R_{exp}(%)			6.20	2.33	2.58	1.96		12.13		16.00
R_B(%)			7.97	5.98	7.28	7.97		8.90		10.56
a(Å)			5.7376(1)	5.6735(2)	5.6782(2)	5.7373(1)		5.6395(2)		5.5895(4)
c(Å)			20.4658(4)	20.3338(5)	20.3987(4)	20.4658(4)		20.3778(6)		20.3414(8)

TABLE II

REFINED ATOMIC POSITIONS AND THERMAL FACTORS (Å²)

Composition:	0.15			0.35			0.5		0.75	
(K):	85	235	585	85	300	585	5	300	85	300
GSS:	*A*2	$P2_1/C$	$R\bar{3}m$	$R\bar{3}m$	$R\bar{3}m$	$R\bar{3}m$	$R\bar{3}m$	$R\bar{3}m$	*C*2/*c*	$R\bar{3}m$
Pb(*1*)										
x	0	0	0	0	0	0	0	0	0	0
y	0	0	0	0	0	0	0	0	0.2883(5)	0
z	0	0	0	0	0	0	0	0	0.25	0
B	0.62(8)	1.30(8)	4.56(16)	2.70(4)	2.76(11)	2.57(14)	2.79(7)	3.29(6)	1.58(6)	2.79(6)
Pb(2)										
x	0.3833(4)	0.3835(5)	0	0	0	0	0	0	0.3160(2)	0
y	0.5499(8)	0.5815(4)	0	0	0	0	0	0	0.3139(3)	0
z	0.2807(3)	0.2879(4)	0.2054(2)	0.2073(3)	0.2069(2)	0.2067(3)	0.2089(2)	0.2092(1)	0.3496(2)	0.2115
B	0.95(6)	0.90(5)	5.44(13)	4.61(13)	4.70(12)	5.27(17)	5.07(9)	4.92(7)	1.63(4)	4.87(7)
P										
x	0.2911(118)	0.2710(74)	0	0	0	0	0	0	0.5991(4)	0
y	0.0156(173)	0.1432(79)	0	0	0	0	0	0	0.2485(11)	0
z	0.3582(95)	0.3009(41)	0.3861(24)	0.3924(13)	0.3954(14)	0.3968(17)	0.3951(4)	0.3957(3)	0.4471(5)	0.3995(2)
B	1.83(15)	1.33(70)	3.72(76)	1.29(29)	2.78(33)	2.95(54)	1.37(13)	1.35(10)	1.10(8)	0.92(6)
V										
x			0	0	0	0		0		0
y	N.R.	N.R.	0	0	0	0	N.R.	0	N.R.	0
z			0.4096(4)	0.4131(18)	0.4094(10)	0.4023(16)		0.4035(8)		0.4014(17)
B			2.05(25)	0.709	4.55(1.10)	5.54(55)		4.82(33)		2.30(80)

TABLE II—*Continued*

Composition:	0.15			0.35			0.5		0.75	
(K):	85	235	585	85	300	585	5	300	85	300
GSS:	*A*2	$P2_1/C$	$R\bar{3}m$	$R\bar{3}m$	$R\bar{3}m$	$R\bar{3}m$	$R\bar{3}m$	$R\bar{3}m$	*C*2/*c*	$R\bar{3}m$
O(1)										
x	0.2398(8)	0.2872(8)	0	0	0	0	0	0	0.6476(3)	0
y	0.2956(11)	0.2559(9)	0	0	0	0	0	0	0.0287(5)	0
z	0.0411(6)	0.0159(7)	0.3235(4)	0.3247(4)	0.3234(3)	0.3246(5)	0.3234(2)	0.3240(2)	0.3847(4)	0.3259(2)
B	1.14(10)	1.45(11)	5.30(17)	3.18(14)	3.39(12)	5.02(10)	2.62(7)	2.79(6)	1.35(2)*	2.17(5)
O(2)										
x	0.2948(8)	0.2598(7)	−0.1584(4)	−0.1567(4)	−0.1572(4)	−0.1565(5)	−0.1552(3)	−0.1556(2)	0.6355(3)	−0.1540(2)
y	0.7251(11)	0.7079(7)	0.1584(4)	0.1567(4)	0.1572(4)	0.1565(5)	0.1552(3)	0.1556(2)	0.4714(6)	0.1540(2)
z	0.0259(6)	0.0216(6)	0.4305(7)	0.4299(2)	0.4301(2)	0.4300(2)	0.4292(1)	0.4296(1)	0.3705(4)	0.4283(1)
B	1.05(10)	0.77(9)	3.66(8)	2.49(7)	2.89(7)	3.51(11)	2.70(7)	2.83(4)	1.35(2)*	2.31(3)
O(3)										
x	0.3265(9)	0.3194(7)							0.6430(3)	
y	0.9533(12)	0.9784(7)							0.2792(5)	
z	0.2943(6)	0.2823(5)							0.6162(3)	
B	1.14(9)	0.96(9)							1.35(2)*	
O(4)										
x	0.0332(6)	0.0335(7)							0.4858(2)	
y	0.5511(12)	0.5431(8)							0.2223(6)	
z	0.2181(5)	0.2091(5)							0.4168(3)	
B	1.12(10)	1.40(11)							1.35(2)*	

Note. N.R. means not refined.

* Refined simultaneously.

TABLE III

BOND LENGTHS (Å) FOR VANADIUM-RICH COMPOUNDS

Composition:	$x = 0(7)$			$x = 0.15$			$x = 0.35$		
Phase:	γ	β	α	γ	β	α	γ	γ	γ
T(K):	585	300	85	585	235	85	585	300	85
Pb(1)									
$O_1'\times2$		2.612(12)	2.449(9)		2.606(13)	2.461(12)			
$O_2'\times2$	2.645(9)	2.599(10)	2.731(11)	2.641(5)	2.575(11)	2.700(13)	2.637(6)	2.624(5)	2.622(7)
$O_3'\times2$		2.757(8)	2.767(10)		2.734(10)	2.763(11)			
Pb(2)									
O_1		2.586(13)	2.986(13)		2.602(16)	2.971(16)			
O_2	2.777(7)	3.378(12)	2.984(15)	2.815(10)	3.380(14)	3.033(17)	2.848(11)	2.834(9)	2.843(11)
O_3		2.628(15)	2.627(18)		2.659(19)	2.616(20)			
O″(1)		3.330(14)	3.321(15)		3.269(18)	3.314(18)			
O″(2)		3.049(15)	3.479(16)		3.024(17)	3.406(19)			
O″(3)	2.953(9)	2.471(7)	2.544(12)	2.937(4)	2.445(10)	2.535(16)	2.911(5)	2.900(3)	2.901(5)
O″(1)		2.416(17)	2.419(18)		2.415(20)	2.418(21)			
O″(2)		3.063(18)	2.516(17)		3.078(20)	2.544(21)			
O″(3)		3.706(7)	3.735(13)		3.677(9)	3.710(15)			
O″(4)	2.416(6)	2.427(14)	2.391(14)	2.417(14)	2.418(15)	2.411(13)	2.413(18)	2.374(12)	2.388(15)
P′									
O‴(1)					1.574(96)	1.861(103)			
O‴(2)				1.818(40)	1.870(90)	1.860(101)	1.686(28)	1.699(23)	1.719(24)
O‴(3)					1.778(98)	1.655(107)			
O′(4)				1.280(64)	1.576(64)	1.461(75)	1.478(51)	1.467(39)	1.376(39)
V′									
O‴(1)		1.708(24)	1.584(25)						
O‴(2)	1.700(17)	1.737(22)	1.940(24)	1.631(9)			1.643(25)	1.601(16)	1.578(22)
O‴(3)		1.716(19)	1.726(26)		N.R.	N.R.			
O′(4)	1.660(20)	1.685(20)	1.699(25)	1.761(18)			1.591(49)	1.753(30)	1.798(50)

Note. N.R. means not refined.

mal factor of all atoms are quite similar to the values generally obtained.

(*a*) *Structural Consequences of the Phosphorus-for-Vanadium Substitution in the Rhombohedral Phase*

Vanadium and phosphorus tetrahedra. In the γ-rhombohedral phase of lead phosphate or lead vanadate the PO_4 or VO_4 tetrahedra are centered on $3m$ symmetry sites: the vanadium or phosphorus atom is bonded to three equivalent oxygen atoms (O_1''', O_2''', O_3'') and by a fourth bonding parallel to the threefold axis to the O′4 atom (Figs. 2 and 3). When making the substitution of vanadium for phosphorus, the two distances O_1'''–O_2''' and O_1'''–O_4' increase linearly (Table II and III); for example the O_1'''–O_2''' bond increases from 2.51 ($x = 1.$) to 2.63 Å ($x = 0.5$) at 300 K and from 2.67 ($x = 0.35$) to 2.78 Å ($x = 0.$) at 585 K. This is consistent with the difference between the ionic radii of the V^{5+} and P^{5+} ions (0.59 and 0.34 Å, respectively). The short O–O bonds in the PO_4 tetrahedra are equivalent to those classically observed in compounds with phosphates tetrahedra (*11*).

When the phosphorus concentration x decreases, the P–O_4' distance with the vertex atom O_4', decreases from 1.464 Å to 1.280 Å

TABLE IV

BOND LENGTHS (Å) FOR PHOSPHORUS-RICH COMPOUNDS

Compounds:	$x = 0.5$		$x = 0.75$		$x = 1$	
Phase:	γ	γ	γ	β'	γ	β'
T(K):	300	5	300	85	473	300
Pb(1)						
$O_1'(\times 2)$				2.571(9)		2.531(24)
$O_2'(\times 2)$	2.628(5)	2.620(7)	2.602(5)	2.691(10)	2.583(18)	2.707(25)
$O_3'(\times 2)$				2.596(7)		2.604(22)
Pb(2)						
O_1				2.720(10)		2.808(35)
O_2	2.891(7)	2.878(7)	2.943(7)	3.221(10)	2.993(32)	3.240(33)
O_3				2.944(10)		2.979(37)
O‴(1)				3.157(7)		3.045(22)
O‴(2)				2.877(8)		2.836(23)
O″(3)				2.418(7)		2.413(26)
O″(1)	2.867(5)	2.881(6)	2.854(5)	2.496(10)	2.816(19)	2.526(33)
O″(2)				2.894(8)		2.994(31)
O″(3)				3.468(6)		3.404(21)
O″(4)	2.342(8)	2.328(9)	2.331(8)	2.359(9)	2.298(36)	2.401(38)
P′						
O‴(1)				1.618(6)		1.487(35)
O‴(2)	1.669(9)	1.671(11)	1.604(7)	1.583(10)	1.538(26)	1.568(34)
O″(3)				1.599(10)		1.557(27)
O′(4)	1.464(13)	1.459(14)	1.499(9)	1.539(12)	1.514(36)	1.473(37)
V′						
O‴(1)						
O‴(2)	1.610(13)	N.R.	1.591(24)	N.R.		
O″(3)						
O′(4)	1.623(23)		1.538(43)			

Note. N.R. means not refined.

whereas the distances with the basal oxygen atoms (P–O_1''' type) increase from 1.538 Å to 1.818 Å (Table III and IV). In the case of the vanadium atoms the precision is not so good but a global decrease of the four bond distances is observed when x increases (Table III and IV).

Lead polyhedra. There are two lead atom sites in the γ structure (Fig. 2). The first one (Pb_1) is a centrosymmetric site ($3m$) situated at the vertices of two tetrahedra with basal oxygen atoms. The Pb_1 polyhedron is therefore characterized by a unique distance (Pb_1–O_1', for example) (Fig. 3). The second one (Pb_2) is bonded (inside the layer of PO_4/VO_4 tetrahedra) to a hexagon built up by six oxygen atoms (for example O_1'') located in a plane orthogonal to the threefold axis, and to an oxygen atom (O_4'') along the threefold axis. It is also bonded to three oxygen atoms of the opposite layer (for example, O_1 in Fig. 3). Thus three distances (Pb_2–O_1'', Pb_2–O_4'', Pb_2–O_1) characterize this second polyhedron in the rhombohedral phase (Fig. 3).

In the γ-phase the Pb_1–O_1' bond lengths are significantly long, in particular in the vanadium-rich compounds. Indeed we observed, for instance, in the $x = 0$ compound Pb_1–O_1' bond lengths of 2.64 Å, whereas in divalent lead polyhedra the Pb–O lengths

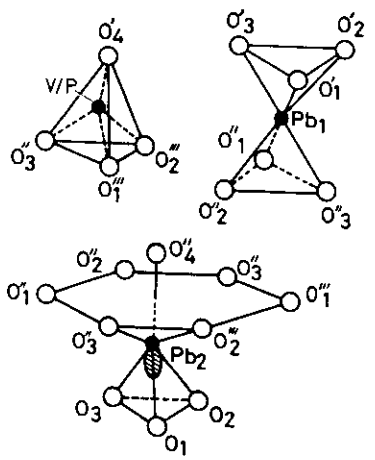

FIG. 3. Polyhedra of Pb_1, Pb_2, and V or P atoms in the γ-phase (from Ref. (7)).

are classically shorter than 2.50 Å. When phosphorus is substituted for vanadium the Pb_1 polyhedron is weakly affected: The Pb_1–O_1' distances decrease linearly from 2.64 to 2.58 Å. In contrast, the distances in the Pb_2 polyhedron show strong variations: when x increases from 0 to 1 the Pb_2–O_1 interlayer bond length increases from 2.78 to 2.99 Å whereas the bond lengths inside the layer (Pb_2–O_1'') decrease from 2.95 to 2.82 Å. Moreover the shortest lead–oxygen distance (Pb_2–O_4'') changes from 2.42 to 2.30 Å. Thus, in lead phosphate the shortest Pb_2–O bonds are intralayer bonds whereas in lead vanadate they are interlayer bonds (Fig. 2, 3). When phosphorus is substituted for vanadium a continuous variation of these bonds is observed and for $x = 0.5$ they become equal.

(*b*) *Phase Transitions in the Mixed Compounds* $Pb_3P_{2x}V_{2(1-x)}O_8$

Transition $\gamma \rightarrow \beta'$. We have performed a more complete analysis of the structural evolution at the γ–β' transition for the phosphorus-rich compound $x = 0.75$. The O_1'''–O_2''' and O_1'''–O_4' distances of the PO_4 tetrahedra, almost equal in the γ phase, display an opposite discontinuity at the transition (Fig. 4). Inside this distorted tetrahedron of oxygen atoms the phosphorus remains practically at the position occupied in the γ-phase: the P–O_1''' type distances split at the transition into three almost equal distances, but all the bondings with the oxygen atoms, including the P–O_4, display no significant variation when the temperature is decreased.

In the Pb_1 polyhedron the six equivalent bond distances (Pb_1–O_1' type) split discontinuously at the critical temperature into three nonequivalent lengths, two of them being almost equal, but with only small thermal variation in the β' phase (Fig. 5).

In the Pb_2 polyhedron the three equivalent bonds with the oxygen atoms O_i of the opposite layer split at the critical temperature into three very different lengths (2.82, 3.00, and 3.14 Å instead of 2.87 Å, Fig. 6); the six equivalent bondings with the hexagon of oxygens inside the layer show the largest discontinuities (2.53, 2.60, 2.84, 2.93, 3.05, and 3.27 Å instead of 2.85 Å) while the shortest bond distance Pb_2–O_4'' displays a small change and remains afterwards almost con-

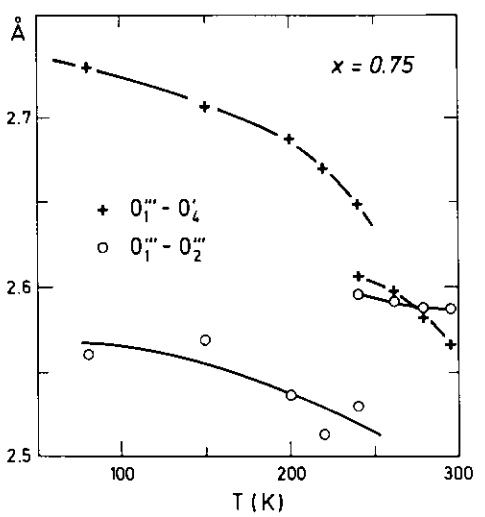

FIG. 4. Thermal evolution of two oxygen–oxygen distances of PO_4 and VO_4 tetrahedra, for the $x = 0.75$ compound.

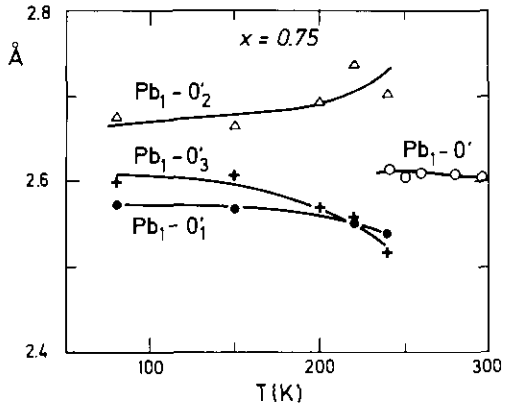

FIG. 5. Thermal evolution of lead–oxygen distances of the Pb_1 polyhedron, for the $x = 0.75$ compound. Below the critical temperature the six equivalent distances of the rhombohedral phase split into three nonequivalent distances in the monoclinic phase.

stant (Fig. 7). Therefore the main distortions in the β' monoclinic phases of mixed compounds lie in the Pb_2 polyhedron whereas the PO_4/VO_4 tetrahedra and the Pb_1 polyhedron are less affected by the transition. The distortions observed in the $x = 0.75$ compound below the critical temperature are equivalent to those observed at room temperature in the monoclinic phase of $Pb_3P_2O_8$ (*8*, *1*).

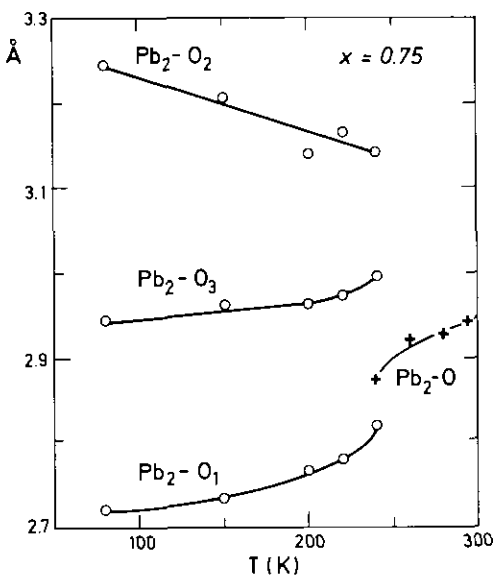

FIG. 6. Thermal evolution of interlayer lead–oxygen distances of the Pb_2 polyhedron, for the $x = 0.75$ compound. Below the critical temperature the three equivalent distances of the rhombohedral phase split into three nonequivalent distances in the monoclinic phase.

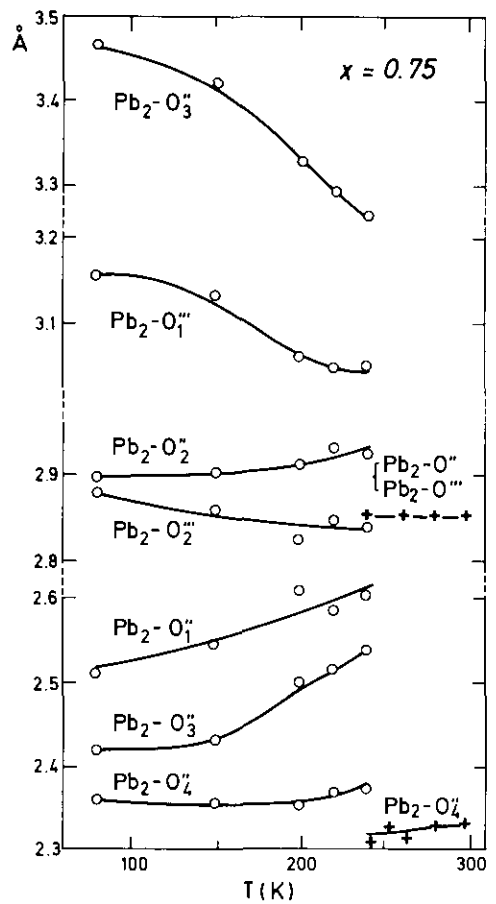

FIG. 7. Thermal evolution of intralayer lead–oxygen distances of the Pb_2 polyhedron, for the $x = 0.75$ compound. Below the critical temperature the six equivalent distances (from the hexagon of oxygen atoms) in the rhombohedral phase split into six nonequivalent distances in the monoclinic phase.

The evolution of the thermal factors is plotted in Fig. 8. The isotropic thermal parameters of the Pb_2 atoms are quite high in the γ-phase at temperatures far from the critical temperature (for example, $B = 5.3$ Å^2 at 300 K). When the temperature de-

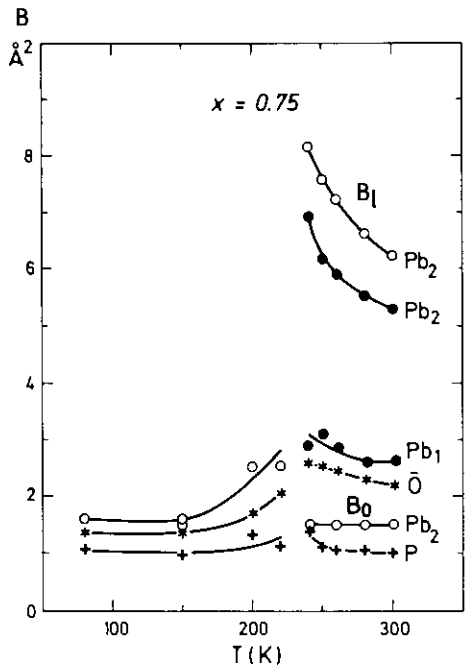

FIG. 8. Thermal evolution of B thermal factors, for the $x = 0.75$ compound. Above the critical temperature the isotropic B factor of the lead Pb_2 atoms has been decomposed into two components: one component $B_\parallel$ inside the layers, and one component B_0 orthogonal to the layers.

creases an increase of all thermal parameters is observed in the vicinity of the critical temperature, especially for the Pb_2 atom. Conversely, below the critical temperature, in the β'-phase, these coefficients diminish and reach usual values. The isotropic parameter of the lead atom Pb_2 has been decomposed into two components: one high value $B_\parallel$ parallel to the layer and one normal value B_0 orthogonal to the layer. It is observed that in the γ-phase only the $B_\parallel$ component gets strong variation whereas the B_0 component remains constant.

Transitions $\gamma \rightarrow \beta \rightarrow \alpha$. The examination of the bond distances (Table III) in the β and α phases of the mixed compound $x = 0.15$ shows the same type of distortions that are observed in $Pb_3V_2O_8$ (7). As in the β'-phase the PO_4 tetrahedron has only small distortions. In the Pb_1 polyhedron, for both $x = 0$ and $x = 0.15$ compounds, the abnormally high Pb–O distances (2.64 Å in the γ-phase) split into three different distances, one of them with more usual values (2.60 Å in the β phase and 2.46 Å in the α-phase).

The intralayer bondings of the lead Pb_2 atom with the hexagon of oxygen display very large variations (for instance, the Pb_2–O_3'' distance changes from 2.93 Å up to 3.67 and 3.71 Å). The high values of B isotropic thermal parameters in the γ-phase recover normal values inside the β phase.

Discussion

Consequences of the substitution for the common γ *phase.* The results show that the substitution of phosphorus for vanadium in the common rhombohedral phase affects principally the PO_4/VO_4 tetrahedra and the Pb_2 polyhedron.

In the PO_4/VO_4 tetrahedra, as the size of the cage of oxygen atoms increases when the concentration of vanadium from lead phosphate is increased, the phosphorus ions shift toward the vertex resulting in one normal bond distance value and three long bond distances. In parallel the vanadium ion keeps a almost constant V–O_4' distances for concentration close to $Pb_3V_2O_8$, but for the phosphorus-rich compounds this is no longer possible because the oxygen cage becomes too small: all the V–O bonding lengths decrease when the phosphorus concentration increases.

In the lead Pb_2 polyhedron the shortest lead–oxygen distance (Pb_2–O_4'') is smaller in lead phosphate than in lead vanadate. Moreover, the oxygen atoms forming a hexagon O_i'' and O_i''' are closer to the lead atom than the three other oxygen O_i atoms of the other layer, whereas it is the opposite in lead vanadate. When x decreases from lead phosphate, the Pb_2–O_4'' and the Pb_2–O_i'' distances continuously increase whereas the Pb_2–O_i' decrease. For $x = 0.5$ both Pb_2–O_i and Pb_2–

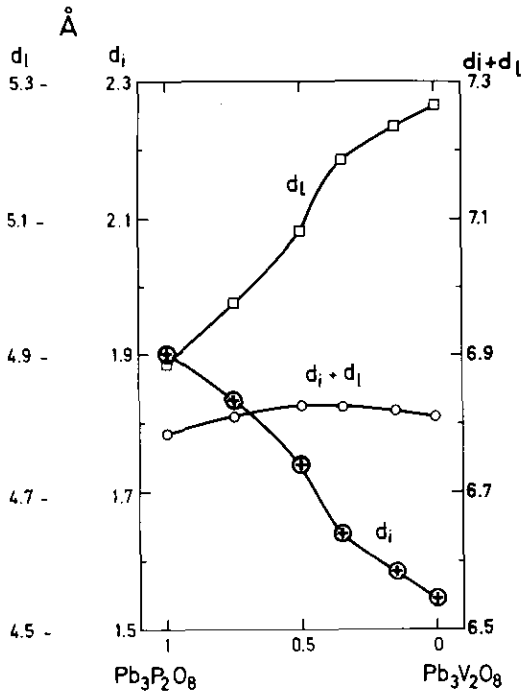

FIG. 9. Evolution with concentration x of the interlayer distance d_l, of the layer distance d_i, and of the distance $d_l + d_i$.

O_i'' distances become equal and in lead vanadate $x = 0$ the Pb_2–O_i' distance has became much shorter than the Pb_2–O_i'' distance.

In lead phosphate and lead vanadate the lone pair of lead is rejected along the threefold axis by the proximate oxygen atoms, mainly because of the short Pb_2–O_4'' bond. In the mixed compounds this lone pair gets a continuous decrease of its spatial extension from $x = 1$ to $x = 0$. This is also evidenced in the variation of the interlayer distance d_i (only occupied by the lone pairs) with the concentration, which diminishes strongly from 1.92 ($x = 1$) to 1.55 Å ($x = 0$) (Fig. 9). Moreover as the skeleton of layers d_l is a stacking of tetrahedra with increasing sizes when x diminishes, this distance strongly increases from $Pb_3P_2O_8$ to $Pb_3V_2O_8$ whereas the total distance $d_l + d_i$ remains relatively constant whatever x is, with a small maximum for $x = 0.5$.

Phase transitions in the mixed system. As in lead vanadate and lead phosphate, the PO_4/VO_4 tetrahedra and the Pb_1 polyhedron are less distorted than the Pb_2 polyhedron in the different monoclinic phases. Moreover the structures of monoclinic phases are only weakly affected by the substitution, as shown by the comparison of the β'-phase of the $x = 1$ and $x = 0.75$ compounds, and the β and α phase of the $x = 0$ and $x = 0.15$ compounds.

As the temperature cools the interlayer distance d_i inside the γ phase diminishes to a limiting value d_i^{min} dependent on the concentration x (Fig. 10). For the compounds whose rhombohedral structure remains stable whatever the temperature is, the shortest interlayer is the value measured at 5 K which is clearly above the extrapolated variation in the medium part of the phase diagram. When this limiting value can be reached a transition toward a monoclinic phase is observed.

Critical region and monoclinic local order in the γ phase. The high values of B thermal

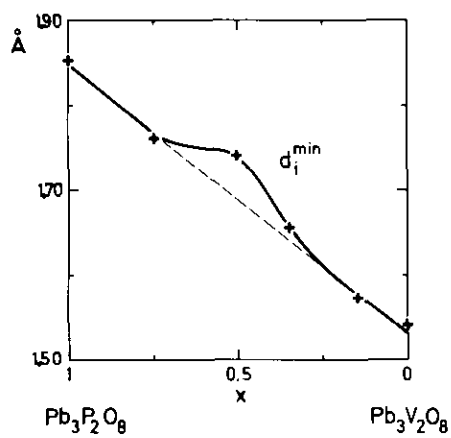

FIG. 10. Evolution with the concentration x of the lowest interlayer distance d_i^{min} value reached inside the γ rhombohedral phase when the temperature is decreased. The values for the compounds whose rhombohedral phase remain stable whatever the temperature is (middle part of the phase diagram) are clearly above the extrapolated values from those of the compounds which get a phase transition from the γ-phase.

parameters of lead atoms in the γ phase, whatever x is, reveal the existence of shifts of these atoms from their high symmetry sites. Depending on the temperature these shifts are static or dynamic. The high values of B observed at 5 K for the concentrations with no phase transition indicate in these cases static displacements which become at least partially dynamic at higher temperature, as an increase in the B factors is observed. Moreover for the compound $x = 0.75$ a supplementary increase is observed in the rhombohedral phase in the vicinity of the critical temperature. This reveals the critical fluctuations of the system: as the main displacements at the different transitions are for the lead Pb_2 atoms inside the layer, coherently their thermal parameter inside the layer B_1 strongly increases near T_c, whereas their orthogonal parameter B_o remains constant. Below this temperature in the monoclinic phases normal B values are recovered.

In the same way the high values of the B parameter for the Pb_1 atoms are the consequence of shifts from their special centrosymmetric sites probably due to the abnormal high value of the Pb_1–O distances in the γ-phase.

All these results probably indicate the existence of a local monoclinic order inside the rhombohedral phase. In the case of compounds which get a phase transition this local order anticipates the monoclinic phase and becomes of long range when the cooperative movements of the lead atoms occur at T_c, as is evidenced in lead phosphate (*5*) and in $Pb_3P_{2x}As_{(1-x)}O_8$ (*12*). For the compounds whose rhombohedral phase remains stable down to low temperature this local order is frozen. This hypothesis is also supported by the increase at low temperature of the R_{wp} reliability factor for the $x = 0.5$ and 0.35 compounds (Table I).

Conclusion

These results allow us to propose a common mechanism for the phase transitions of lead orthophosphovanadates. When the temperature is decreased inside the high temperature γ-phase, the interlayer distance between the lead atoms diminishes down to a critical value. If this critical value can be reached, then the lone pairs tilt in order to minimize these repulsions and a phase transition with strong shears toward a monoclinic phases occurs, as for lead phosphate and lead vanadate; in the other cases the rhombohedral phase remains stable at low temperatures.

Acknowledgments

The authors thank B. Rieu for his kind assistance during the neutron experiments.

References

1. J. M. Kiat, Y. Yamada, G. Chevrier, Y. Uesu, P. Boutrouille, and G. Calvarin, *J. of Phys. C* **4**, 4915 (1992).
2. P. Garnier, G. Calvarin, J.-F. Berar, and D. Weigel, *Mater. Res. Bull.* **19**, 407 (1984).
3. H. Kasatani, T. Umeki, H. Terauchi, and Y. Ishibashi, *J. Phys. Soc. Jpn.* **60**, 1169 (1991).
4. J. M. Kiat, G. Calvarin, P. Garnier, and P. Gregoire, *J. Phys.* **48**, 253 (1987).
5. J. M. Kiat, G. Calvarin, and Y. Yamada, to be published in *Phys. Rev. B*.
6. Y. Yamada, Y. Noda, M. Takimoto, and K. Furukawa, *J. Phys. Soc. Jpn.* **54**, 2940 (1985).
7. J. M. Kiat, P. Garnier, and M. Pinot, *J. Solid State Chem.* **91**, 339 (1991).
8. D. M. C. Guimaraes, *Acta Crystallogr. Sect. A.* **35**, 108 (1979).
9. J. F. Berar, G. Calvarin, and D. Weigel, *J. Appl. Crystallogr.* **13**, 201 (1980).
10. D. B. Wiles and R. A. Young, *J. Appl. Crystallogr.* **14**, 149 (1981).
11. S. Haussühl, B. Middendorf, and M. Dörffel, *J. Solid State Chem.* **93**, 9 (1991).
12. E. Salje and B. Wruck, *Phys. Rev. B* **28**(11), 6510 (1983).